Zhang *et al. Chem Synth* 2023;3:5
DOI: 10.20517/cs.2022.28

Chemical Synthesis

Research Article

Open Access

Lysine-modulated synthesis of enzyme-embedded hydrogen-bonded organic frameworks for efficient carbon dioxide fixation

Boyu Zhang[1], Jiafu Shi[1,2,3,*], Ziyi Chu[1], Jiaxu Zhang[1], Zhenhua Wu[1], Dong Yang[1], Hong Wu[2,4], Zhongyi Jiang[2,4,*]

[1]School of Environmental Science & Engineering, Tianjin University, Tianjin 300072, China.
[2]Collaborative Innovation Center of Chemical Science and Engineering (Tianjin), Tianjin 300072, China.
[3]State Key Laboratory of Biochemical Engineering, Institute of Process Engineering, Chinese Academy of Sciences, Beijing 10090, China.
[4]Key Laboratory for Green Chemical Technology of Ministry of Education, School of Chemical Engineering and Technology, Tianjin University, Tianjin 300072, China.

Correspondence to: Prof. Jiafu Shi, School of Environmental Science & Engineering, Tianjin University, 92 Weijin Road, Tianjin 300072, China. E-mail: shijiafu@tju.edu.cn; Prof. Zhongyi Jiang, School of Chemical Engineering & Technology, Tianjin University, 92 Weijin Road, Tianjin 300072, China. E-mail: zhyjiang@tju.edu.cn.

How to cite this article: Zhang B, Shi J, Chu Z, Zhang J, Wu Z, Yang D, Wu H, Jiang Z. Lysine-modulated synthesis of enzyme-embedded hydrogen-bonded organic frameworks for efficient carbon dioxide fixation. *Chem Synth* 2023;3:5. https://dx.doi.org/10.20517/cs.2022.28

Received: 16 Sep 2022 **First Decision:** 17 Nov 2022 **Revised:** 4 Jan 2023 **Accepted:** 11 Jan 2023 **Published:** 17 Jan 2023

Academic Editors: Bao-Lian Su, Damien P. Debecker **Copy Editor:** Ke-Cui Yang **Production Editor:** Ke-Cui Yang

Abstract

Carbonic anhydrase (CA) is an important carbon fixation enzyme. Immobilization of CA can expand its application in the realm of adsorption, catalysis, and so on. As a typical metal-free framework, hydrogen-bonded organic frameworks (HOFs) featuring mild synthesis process, exquisite framework structure and good enzyme compatibility have been used for enzyme embedding. However, the catalytic performance of CA-embedded HOFs (CA@HOFs) is limited by the micropore size of HOFs and the slow adsorption of CO_2. Herein, CA@Lys-HOF-1 was synthesized by introducing lysine (Lys), a basic amino acid, during the coprecipitation of CA and HOFs for CO_2 fixation. The addition of Lys enlarged the average pore size of HOF-1 from 1.8 to 3.2 nm, whereas the introduced -NH_2 groups increased the initial adsorption of CO_2 from 0.55 to 1.21 cm^3 g^{-1}. Compared to CA@HOF-1, the activity of CA@Lys-HOF-1 was enhanced by 71.25%, and the corresponding production of $CaCO_3$ was enhanced by 12.7%. After eight reaction cycles, CA@Lys-HOF-1 still maintained an output of 9.97 mg of $CaCO_3$ every 5 min, 83.7% of the initial production. It is hoped that the CA@Lys-HOF-1 reported offers a platform for efficient and continuous fixation of CO_2.

Keywords: Carbon dioxide fixation, carbonic anhydrase, hydrogen-bonded organic frameworks, enzyme catalysis, enzyme immobilization

INTRODUCTION

Carbon dioxide (CO_2) capture and utilization (CCU) is one of the ever-increasing research topics which can contribute to addressing environmental and ecological issues[1-4]. Enzymes such as formate dehydrogenase (FDH), ribulose-1, 5-bisphosphate carboxylase/oxygenase (RubisCO), and carbonic anhydrase (CA) can accurately activate CO_2 to lower the reaction energy barrier, which have received great attention as a green and feasible solution to CCU[5-7]. CA exhibits the highest catalytic rate among all carbon-fixation enzymes, and thus has good potential for the selective transformation of CO_2 to HCO_3^-[8]. However, enzymes that leave the bodies of organisms are easy to inactivate and difficult to reuse[9-11]. One frequently used method to address the above issues is to immobilize enzymes inside carrier materials[12].

Porous framework materials, such as metal-organic frameworks (MOFs)[13-17], covalent organic frameworks (COFs)[18-22], and hydrogen-bonded organic frameworks (HOFs)[23-25], bearing high specific surface area, high porosity, exquisite framework structure and excellent designability, are emerging carriers for enzyme immobilization. Particularly, HOFs are framework materials linked by hydrogen bonds[26-29], which can be reversibly repaired by simple recrystallization[30,31] and possess better biocompatibility due to the absence of metal ions[32,33]. These advantages make HOFs an excellent candidate as enzyme immobilization carriers[34]. For example, HOF-21 synthesized by Bao *et al*. can recover its original structure after immersion in aqueous or anionic source solution for 48 h[35]. Tang *et al.* designed TA-HOFs capable of *in situ* embedding enzymes with different surface charges and molecular weights[36]. Enzyme in TA-HOFs exhibited remarkably enhanced stability. However, HOFs with micropore size and balanced -NH_2/-COOH groups usually showed restricted mass transfer and lower affinity with CO_2, therefore exhibiting reduced apparent enzyme activity.

Herein, HOF-1 composed of two units of Tetrakis(4-amidiniumphenyl)methane and tetrakis (4-carboxyphenyl) methane was selected for CA embedding[37]. The structure of HOF-1 was modulated by introducing basic amino acids during the synthesis process. Briefly, carbonic anhydrase@HOF-1 (CA@HOF-1) was prepared by a coprecipitation method, in which CA was *in situ* embedded. The structure of CA@HOF-1 was modulated by altering the species and amount of amino acid. We found that basic amino acids, especially lysine (Lys), can interact with the carboxyl monomer of HOF-1 to occupy some of the hydrogen bond formation sites, thus causing defects of HOF-1 to promote mass transfer. Meanwhile, the introduced -NH_2 groups also facilitated the initial adsorption of CO_2. Compared to CA@HOF-1, CA@Lys-HOF-1 showed a 12.7% enhancement in CO_2 fixation efficiency. When CO_2 was introduced at a flow rate of 25 mL min^{-1}, $CaCO_3$ precipitation reached 12.26 mg after 5 min of ventilation. After 8 cycles, CA@Lys-HOF-1 maintained an output of 9.97 mg $CaCO_3$ every 5 min. It is believed that Lys-HOF-1 is an ideal framework material for CO_2-converting enzyme embedding.

EXPERIMENTAL

Materials and chemicals

Tetrakis(4-amidiniumphenyl)methane tetrahydrochloride (TAM, 95%) was purchased from Jilin Chinese Academy of Sciences-Yanshen Technology Co., Ltd. Tetrakis(4-carboxyphenyl)methane ($C_{29}H_{20}O_8$, 98%) was obtained from Shanghai Macklin Biochemical Technology Co., Ltd. γ-poly-l-glutamic acid (PLGA, 92%), glycine ($C_2H_5NO_2$, 98%), serine ($C_3H_7NO_3$, 98%), arginine ($C_6H_{14}N_4O_2$, 98%), and lysine ($C_6H_{14}N_2O_2$, 98%) were obtained from Shanghai Aladdin Bio-Chem Technology Co., Ltd. Carbonic anhydrase (EC 4.2.1.1) was acquired from Sigma-Aldrich Co., Ltd. All other chemicals were used as received without any purification.

Synthesis of HOF-1

Tetrakis(4-amidiniumphenyl)methane tetrahydrochloride (10 mg) was dissolved in H_2O (2.5 mL) to form solution A. Tetrakis(4-carboxyphenyl)methane (7.5 mg) was dispersed in H_2O (2375 μL), followed by the addition of aqueous ammonium hydroxide solution (1% v/v, 125 μL) to form solution B. Thereafter, solution B was added to solution A under stirring conditions at room temperature. Precipitation occurred immediately upon mixing. The reaction mixture was left to stir gently in the dark for 1 h. The HOF-1 material was then recovered by centrifugation, washed, dispersed, and centrifuged three times in H_2O to remove any unreacted precursors.

Synthesis of CA@HOF-1

Tetrakis(4-amidiniumphenyl)methane tetrahydrochloride (10 mg) was dissolved in H_2O (1.25 mL) to form solution A. An aqueous solution of CA (1.25 mL of 2 mg mL^{-1} stock solution) was added to solution A and stirred at room temperature for 10 min to form solution B. Tetrakis(4-carboxyphenyl)methane (7.5 mg) was dissolved in 2375 μL of H_2O and 125 μL of 1% NH_4OH to form solution C. Solution C was then added dropwise to solution B under stirring. The mixture was then left to stir gently for another 1 h to ensure the completion of the synthesis. Thereafter, CA@HOF-1 was collected by centrifugation and then washed, dispersed, and centrifuged three times in H_2O to remove the unreacted precursors and loosely adsorbed CA.

Synthesis of CA@amino acid-HOF-1

Tetrakis (4-carboxyphenyl) methane (7.5 mg) was dissolved in 2375 μL of H_2O and 125 μL of 1% NH_4OH to form solution A. An aqueous solution of CA (0.625 mL of 4 mg mL^{-1} stock solution) and amino acid (0.625 mL of 1/10/20 mg mL^{-1} stock solution) was added to solution A and stirred at room temperature for 10 min to form solution B. Tetrakis(4-amidiniumphenyl)methane tetrahydrochloride (10 mg) was dissolved in H_2O (1.25 mL) to form solution C. Solution C was then added dropwise to solution B under stirring. The mixture was then left to gently stir for another 1 h to ensure the completion of the synthesis. Thereafter, CA@amino acid-HOF-1 was collected by centrifugation and then washed, dispersed, and centrifuged three times in H_2O to remove any unreacted precursors and loosely adsorbed CA.

Characterization

The sample morphologies were analyzed by scanning electron microscopy (SEM, S-4800, Hitachi) and transmission electron microscopy (TEM, JEM-100CX II, JEOL). The chemical compositions of the samples were identified by Fourier transform infrared (FTIR) spectrometer (Nicolet-6700, Nicolet). The crystal structures of the samples were identified by X-ray diffraction (XRD, X' Pert Pro), with 2-theta ranging from 10° to 90° by a step width of 0.033° with 15.24° min^{-1} speed at 40 mA and 40 kV. The specific surface area and pore size distribution of the samples were examined by Brunauer-Emmett-Teller (BET) method based on N_2 adsorption/desorption isotherms on an AUTOSORB-1 surface area and pore size analyzer (Quantachrome Instruments).

Conversion of CO_2

CA@HOF-1 and CA@Lys-HOF-1 were used for the conversion of CO_2. In a typical experiment, nitrogen was first injected into the aqueous phase of the reaction device for 10 min to remove CO_2 gas in the solution. Then, CO_2 with a rate of 25 mL min^{-1} was injected into the system. A sample was taken every 5 min for follow-up reaction. Specifically, pH value of the reaction solution was detected by a pH meter and kept at 7.9, which was adjusted by adding 5 mol L^{-1} NaOH. Then, a certain amount of reaction solution was mixed with 670 mmol L^{-1} calcium chloride solution. The mixture was shaken at 200 r min^{-1} to form $CaCO_3$ precipitate. The precipitated $CaCO_3$ was filtered by a filter paper with an average pore diameter of 2.5 μm, which was then dried overnight and weighed to determine the relative yield of $CaCO_3$.

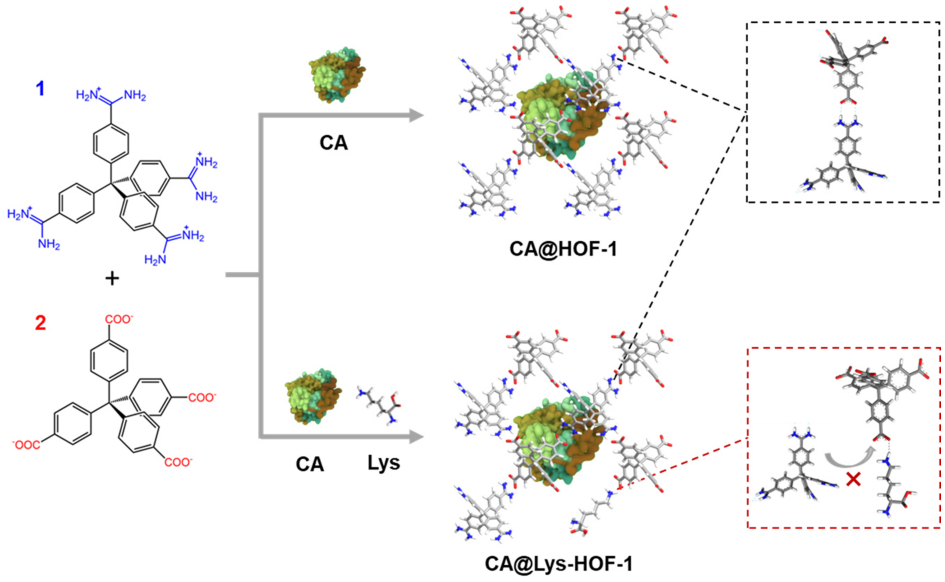

Figure 1. Schematic showing the preparation process of CA@HOF-1 and CA@Lys-HOF-1.

RESULTS AND DISCUSSION

Preparation and Characterization of CA@HOF-1 and CA@Lys-HOF-1

A reported HOF material (HOF-1) was chosen for the embedding of CA[37]. The preparation and structure regulation of CA@HOF-1 are shown in Figure 1. Briefly, HOF-1 was prepared by mixing tetrakis (4-amidiniumphenyl)methane tetrahydrochloride (monomer 1) solution and tetrakis(4-carboxyphenyl) methane (monomer 2) solution under stirring at room temperature [Supplementary Figure 1]. CA@Lys-HOF-1 was prepared by introducing CA and lysine (Lys) during the HOF-1 synthesis process. For control, CA@HOF-1 was also prepared by only adding CA in the HOF-1 synthesis. In advance of the discussion about CA@HOF-1 and CA@Lys-HOF-1, the chemical composition and physical structure of HOF-1 were characterized by FTIR, XRD and ^{13}C-NMR, which are shown in Supplementary Figures 2 and 3.

The topological structures of all samples were also examined by SEM and TEM. As shown in Figure 2 and Supplementary Figure 4, both CA@HOF-1 and CA@Lys-HOF-1 maintain the rod-like structure of HOF-1 with similar dimensions (around 300 nm wide). This indicates that the incorporation of CA and Lys did not alter the structure and size of HOF-1 during crystallization. As depicted in Figure 2C, some defects can be observed on the surface of CA@Lys-HOF-1, while CA@HOF-1 and HOF-1 remain intact. Figure 2D further shows that CA@HOF-1 and CA@Lys-HOF-1 well maintain the crystal structure of HOF-1 with the characteristic peaks at 2θ values of 8.6°, and 17.4°. The results of FTIR analysis of CA@HOF-1 and CA@Lys-HOF-1 are shown in Figure 2E. The absorption band centered at around 1030 cm^{-1} may be assigned to the N-H bending vibration of amide in Lys, indicating the introduction of Lys into HOF-1. To reveal the variation of surface area and pore size distribution of HOF-1 after modulation and enzyme embedding, the N_2 adsorption-desorption isotherms of HOF-1, CA@HOF-1, and CA@Lys-HOF-1 were examined [Supplementary Figure 5]. As shown in Figure 2F and Table 1, CA@Lys-HOF-1 shows a larger pore size and broader size distribution, which may facilitate the transfer of CO_2 from the particle surface to CA. CA@Lys-HOF-1 also has a larger surface area due to the defects caused by Lys, which provides more sites for CO_2 conversion. Then, the CO_2 adsorption tests were performed and the results are shown in Figure 2G and

Table 1. BET analysis and initial CO_2 adsorption volume of HOF-1, CA@HOF-1, and CA@Lys-HOF-1

	HOF-1	CA@HOF-1	CA-Lys@HOF-1
Surface area ($m^2 g^{-1}$)	13.1	14.9	19.7
Main pore diameter (nm)	1.8	3.0	3.2
Initial CO_2 adsorption volume ($cm^3 g^{-1}$)	-0.025	0.546	1.214

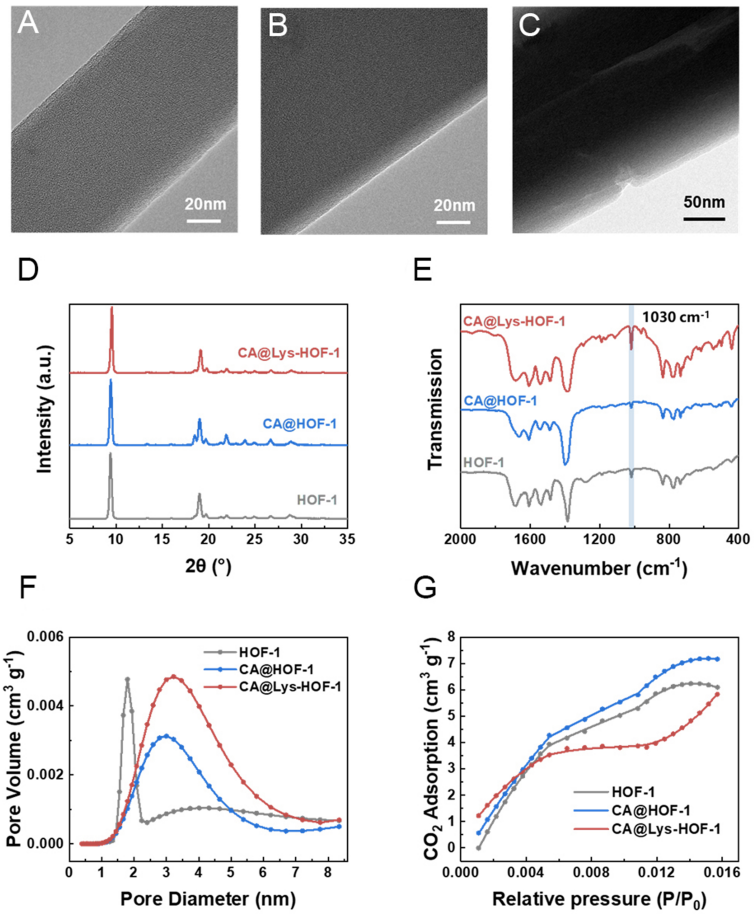

Figure 2. TEM images of (A) HOF-1; (B) CA@HOF-1; and (C) CA@Lys-HOF-1; (D) XRD patterns; (E) FTIR spectra; (F) pore size distribution; and (G) CO_2 adsorption capacity of HOF-1, CA@HOF-1, and CA@Lys-HOF-1.

Supplementary Figure 6. The CO_2 adsorption of CA@Lys-HOF-1 is higher when the CO_2 partial pressure is low, a result due to the relatively larger pore size. With an increase in CO_2 partial pressure, CA@Lys-HOF-1 reaches CO_2 adsorption saturation most quickly, mainly owing to the higher amount of -NH_2 with high CO_2 affinity on the particle surface. As the pressure continued to increase, the final amount of CO_2 adsorption of CA@Lys-HOF-1 was close to that of HOF-1 and CA@HOF-1.

Subsequently, EDS mapping was performed to further investigate whether enzymes were embedded in HOF-1. As shown in Figure 3, the distribution of C and N (the main elements in the two monomers of HOF-1) match the morphology of materials, which can also prove the successful synthesis of HOF-1. Particularly, S (the characteristic element of CA) is uniformly dispersed in the two samples of CA@HOF-1 and CA@Lys-HOF-1, indicating the successful embedding of CA.

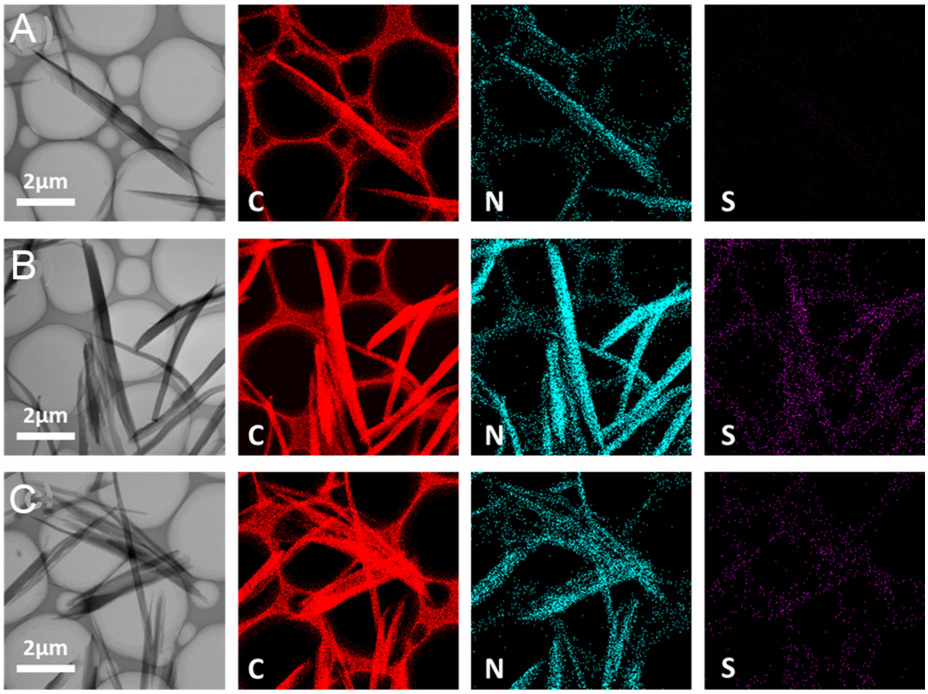

Figure 3. Bright-field images (left) and EDS elemental mapping (right) of C, N, and S for (A) HOF-1; (B) CA@HOF-1; and (C) CA@Lys-HOF-1.

Catalytic activity of CA@Lys-HOF-1

In this work, five different types of (poly) amino acids [Supplementary Figure 7] were adopted to regulate the structure and catalytic performance of CA@HOF-1. Specifically, the hydrogen bonds in HOF-1 are formed between -NH_2 and -COOH of the two monomers, while amino acids are organic compounds containing both -NH_2 and -COOH in the molecule. Amino acids may occupy part of the hydrogen bond formation site, and interfere with the synthesis of HOF-1 through competitive ligand interaction, thus altering the pore size of HOF-1 and influencing the mass transfer.

When γ-poly-l-glutamic acid (PLGA) was introduced, its -COOH groups can rapidly bind to monomer 1, inhibiting the formation of HOF-1. [Supplementary Figure 8]. This was probably due to the preferential combination of -COOH in PLGA and -NH_2 in monomer. Among the other four types of amino acid-modulated CA@HOF-1, the CA@Lys-HOF-1 exerted the highest activity [Supplementary Figures 9 and 10].

The catalytic activity of HOF-1, Lys-HOF-1, CA@HOF-1, and CA@Lys-HOF-1 were tested by dispersing them individually in solution for CO_2 conversion. The activity was reflected by detecting the pH change in the solution after the ventilation of CO_2. The solution without catalyst samples was chosen as control, the Δ pH was measured in real-time, and the value at the highest point was chosen to reflect the catalyst activity. Figure 4A and B shows that the activity of CA@Lys-HOF-1 was enhanced. The higher activity of CA@Lys-HOF-1 may be attributed to the defects resulting from Lys, which promoted mass transfer. The -NH_2 groups in Lys were also introduced into the material, which fortified the affinity between the materials and CO_2 [Supplementary Figure 11]. Furthermore, we investigated the effect of Lys concentrations on the activity. As seen in Figure 4C and D, moderate concentration of Lys is favorable for HOF-1 modulation, thus acquiring the most active CA@Lys-HOF-1. It should be noted that the results of Arg modulation are shown in Supplementary Figure 12, which also shows the same result.

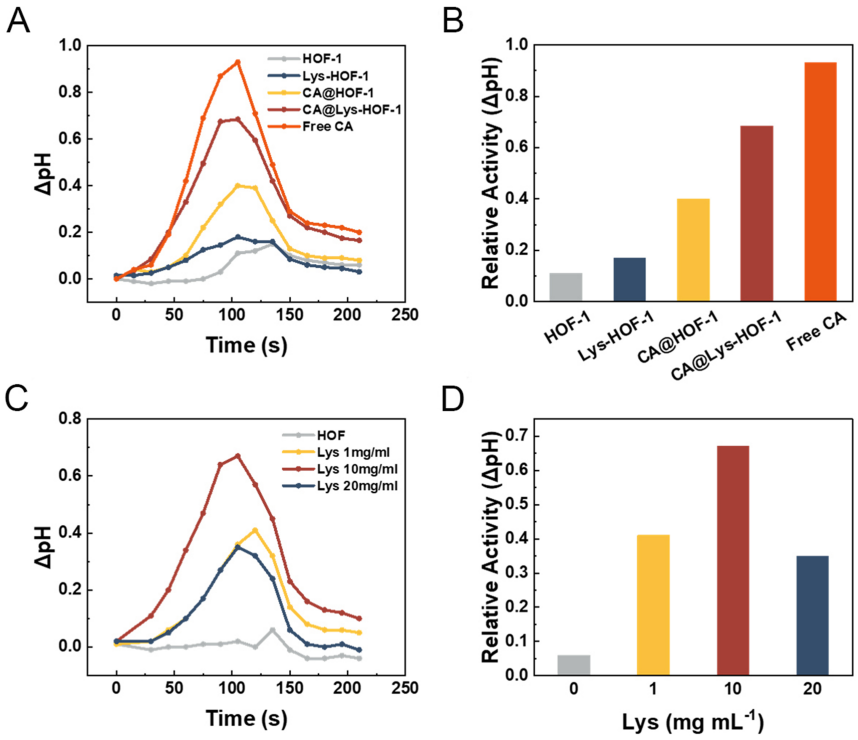

Figure 4. (A and B) Catalytic activity of HOF-1, Lys-HOF-1, CA@HOF-1, CA@Lys-HOF-1, and Free CA; (C and D) Catalytic activity of CA@HOF-1 modulated by different concentrations of Lys.

Stability and CO_2 fixation ability of CA@Lys-HOF-1

Subsequently, the stability, reusability, and CO_2 fixation ability of CA@Lys-HOF-1 were investigated. As shown in Figure 5, Lys-HOF-1 exhibits better protection of CA at different pH values. Regarding the thermal stability, the protective ability of Lys-HOF-1 for CA began to decrease when the temperature was higher than 60 °C. This may be owing to the weakened strength of hydrogen bonds within the carrier material after Lys modification, which made Lys-HOF-1 more prone to decomposition at higher temperatures. The reusability of CA@Lys-HOF-1 was also evaluated for its importance in industrial applications. As shown in Figure 5C, CA@Lys-HOF-1 shows excellent recyclability. After the 8th cycle of reaction, CA@Lys-HOF-1 still maintained 83.7% of its initial activity, and demonstrated unaltered morphological and crystal structure [Supplementary Figure 13].

Finally, to examine the CO_2 fixation ability of CA@Lys-HOF-1, CO_2 was introduced at a flow rate of 25 mL min^{-1}, and the $CaCO_3$ mineralization reaction was performed after 5 min of ventilation. In detail, the reaction rates of the four samples, including HOF-1, Lys-HOF-1, CA@HOF-1, and CA@ Lys-HOF-1, were assessed by measuring the amount of $CaCO_3$ precipitate produced. As shown in Figure 5D, the $CaCO_3$ precipitate amount of HOF-1, Lys-HOF-1, CA@HOF-1, and CA@Lys-HOF-1 is, respectively, 4.81 mg, 6.29 mg, 10.88 mg, 12.26 mg. The production of $CaCO_3$ enabled by CA@Lys-HOF-1 was the highest, again validating the superiority of CA@Lys-HOF-1 in fortifying CO_2 fixation processes. Moreover, a hot filtration[38] experiment was performed over CA@Lys-HOF-1 for CO_2 mineralization. As shown in Supplementary Figure 14, no more increment in the production of $CaCO_3$ is observed after the filtration process, suggesting the heterogeneous nature of our catalytic system.

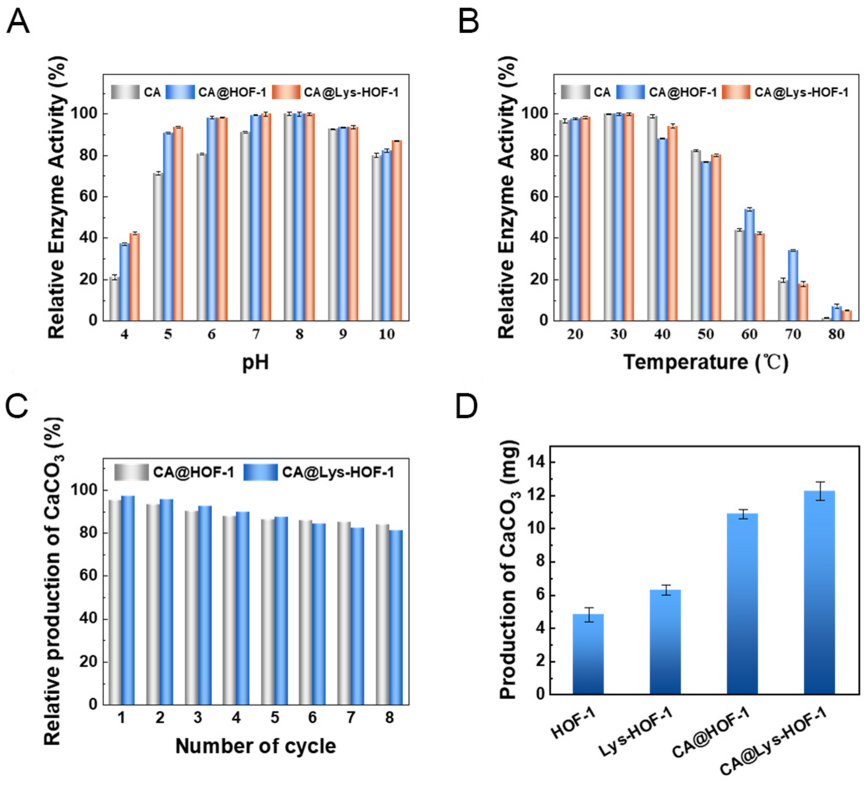

Figure 5. (A) pH stability; (B) thermal stability; (C) reusability; and (D) production of $CaCO_3$ enabled by CA@Lys-HOF-1.

CONCLUSIONS

In summary, HOF-1 modulated by amino acids was synthesized through a coprecipitation method for CA immobilization. By regulating the type and concentration of introduced amino acids, CA@Lys-HOF-1 with optimized activity and desirable stability was obtained. Compared with unmodulated CA@HOF-1, the activity of CA@Lys-HOF-1 was enhanced by 71.3%, whereas the CO_2 fixation efficiency reflected by $CaCO_3$ production was enhanced by 12.7%. This could be ascribed to the large pore size of CA@Lys-HOF-1 that facilitated CO_2 transfer as well as the abundant surface -NH_2 groups that promoted CO_2 adsorption. Moreover, CA@Lys-HOF-1 maintained over 80% of the initial activity after the 8th cycle reaction. Our findings may pave the way for the immobilization of CA and other CO_2-fixation enzymes.

DECLARATIONS

Authors' contributions

Carried out the catalyst preparation, characterization, and catalytic tests, and prepared the draft manuscript: Zhang B

Performed part of the catalyst characterization: Chu Z, Zhang J, Wu Z

Performed the TEM characterization: Yang D, Wu H

Planned the study, analyzed the data and wrote the manuscript: Shi J, Jiang Z

Availability of data and materials

All data needed to evaluate the conclusions in the paper are present in the paper and/or the Supplementary Materials.

Financial support and sponsorship

This work was supported by the National Key R&D Program of China (2022YFC2105902), the National Key R&D Program of China (2021YFC2102300), the National Natural Science Funds of China (22122809), Open Funding Project of the State Key Laboratory of Biochemical Engineering (2020KF-06), and Tianjin Synthetic Biotechnology Innovation Capacity Improvement Project (TSBICIP-KJGG-003) for financial support.

Conflicts of interest

All authors declared that there are no conflicts of interest.

Ethical approval and consent to participate

Not applicable.

Consent for publication

Not applicable.

REFERENCES

1. Yaashikaa P, Senthil Kumar P, Varjani SJ, Saravanan A. A review on photochemical, biochemical and electrochemical transformation of CO_2 into value-added products. *J CO2 Util* 2019;33:131-47. DOI
2. Zhao T, Feng G, Chen W, et al. Artificial bioconversion of carbon dioxide. *Chinese J Catal* 2019;40:1421-37. DOI PubMed
3. Markewitz P, Kuckshinrichs W, Leitner W, et al. Worldwide innovations in the development of carbon capture technologies and the utilization of CO_2. *Energy Environ Sci* 2012;5:7281. DOI
4. Hermida-Carrera C, Kapralov MV, Galmés J. Rubisco catalytic properties and temperature response in crops. *Plant Physiol* 2016;171:2549-61. DOI PubMed PMC
5. Cummins PL, Kannappan B, Gready JE. Directions for optimization of photosynthetic carbon fixation: RuBisCo's efficiency may not be so constrained after all. *Front Plant Sci* 2018;9:183. DOI PubMed PMC
6. Itakura AK, Chan KX, Atkinson N, et al. A Rubisco-binding protein is required for normal pyrenoid number and starch sheath morphology in *Chlamydomonas reinhardtii*. *Proc Natl Acad Sci USA* 2019;116:18445-54. DOI PubMed PMC
7. Valegård K, Andralojc PJ, Haslam RP, et al. Structural and functional analyses of Rubisco from arctic diatom species reveal unusual posttranslational modifications. *J Biol Chem* 2018;293:13033-43. DOI PubMed PMC
8. Lindskog S, Coleman JE. The catalytic mechanism of carbonic anhydrase. *Proc Natl Acad Sci USA* 1973;70:2505-8. DOI
9. Cao S, Yue D, Li X, et al. Novel nano-/micro-biocatalyst: soybean epoxide hydrolase immobilized on UiO-66-NH_2 MOF for efficient biosynthesis of enantiopure (*R*)-1, 2-octanediol in deep eutectic solvents. *ACS Sustain Chem Eng* 2016;4:3586-95. DOI
10. Cao S, Xu P, Ma Y, et al. Recent advances in immobilized enzymes on nanocarriers. *Chinese J Catal* 2016;37:1814-23. DOI
11. Cao S, Xu H, Lai L, et al. Magnetic ZIF-8/cellulose/Fe_3O_4 nanocomposite: preparation, characterization, and enzyme immobilization. *Bioresour Bioprocess* 2017;4:1-7. DOI
12. Alizadeh N, Salimi A, Hallaj R, Fathi F, Soleimani F. Ni-hemin metal-organic framework with highly efficient peroxidase catalytic activity: toward colorimetric cancer cell detection and targeted therapeutics. *J Nanobiotechnology* 2018;16:93. DOI PubMed PMC
13. Drout RJ, Robison L, Farha OK. Catalytic applications of enzymes encapsulated in metal-organic frameworks. *Coord Chem Rev* 2019;381:151-60. DOI
14. Wu X, Hou M, Ge J. Metal-organic frameworks and inorganic nanoflowers: a type of emerging inorganic crystal nanocarrier for enzyme immobilization. *Catal Sci Technol* 2015;5:5077-85. DOI
15. Doonan C, Riccò R, Liang K, Bradshaw D, Falcaro P. Metal-organic frameworks at the biointerface: synthetic strategies and applications. *Acc Chem Res* 2017;50:1423-32. DOI PubMed
16. Riccò R, Liang W, Li S, et al. Metal-organic frameworks for cell and virus biology: a perspective. *ACS Nano* 2018;12:13-23. DOI PubMed
17. Du Y, Gao J, Zhou L, et al. MOF-based nanotubes to hollow nanospheres through protein-induced soft-templating pathways. *Adv Sci (Weinh)* 2019;6:1801684. DOI PubMed PMC
18. Sun Q, Fu CW, Aguila B, et al. Pore environment control and enhanced performance of enzymes infiltrated in covalent organic frameworks. *J Am Chem Soc* 2018;140:984-92. DOI PubMed
19. Serre C, Kitagawa S, Dietzel PD. Introduction to special issue: metal organic frameworks. *Microporous Mesoporous Mater* 2012;157:1-2. DOI

20. Furukawa H, Cordova KE, O'Keeffe M, Yaghi OM. The chemistry and applications of metal-organic frameworks. *Science* 2013;341:1230444. DOI
21. Eum K, Jayachandrababu KC, Rashidi F, et al. Highly tunable molecular sieving and adsorption properties of mixed-linker zeolitic imidazolate frameworks. *J Am Chem Soc* 2015;137:4191-7. DOI PubMed
22. Zhang H, Hou J, Hu Y, et al. Ultrafast selective transport of alkali metal ions in metal organic frameworks with subnanometer pores. *Sci Adv* 2018;4:eaaq0066. DOI PubMed PMC
23. Luo J, Wang J, Zhang J, Lai S, Zhong D. Hydrogen-bonded organic frameworks: design, structures and potential applications. *CrystEngComm* 2018;20:5884-98. DOI
24. Lin RB, He Y, Li P, Wang H, Zhou W, Chen B. Multifunctional porous hydrogen-bonded organic framework materials. *Chem Soc Rev* 2019;48:1362-89. DOI PubMed
25. Hisaki I, Xin C, Takahashi K, Nakamura T. Designing hydrogen-bonded organic frameworks (HOFs) with permanent porosity. *Angew Chem Int Ed Engl* 2019;58:11160-70. DOI PubMed
26. Luzuriaga MA, Benjamin CE, Gaertner MW, et al. ZIF-8 degrades in cell media, serum, and some-but not all-common laboratory buffers. *Supramol Chem* 2019;31:485-90. DOI
27. Velásquez-hernández MDJ, Ricco R, Carraro F, et al. Degradation of ZIF-8 in phosphate buffered saline media. *CrystEngComm* 2019;21:4538-44. DOI
28. Luzuriaga MA, Welch RP, Dharmarwardana M, et al. Enhanced Stability and controlled delivery of MOF-encapsulated vaccines and their immunogenic response in vivo. *ACS Appl Mater Interf* 2019;11:9740-6. DOI PubMed
29. Sun CY, Qin C, Wang XL, et al. Zeolitic Imidazolate framework-8 as efficient pH-sensitive drug delivery vehicle. *Dalton Trans* 2012;41:6906-9. DOI PubMed
30. Persico F, Wuest JD. Use of hydrogen bonds to control molecular aggregation. Behavior of a self-complementary dipyridone designed to self-replicate. *J Org Chem* 1993;58:95-9. DOI
31. Russell VA, Evans CC, Li W, Ward MD. Nanoporous molecular sandwiches: pillared two-dimensional hydrogen-bonded networks with adjustable porosity. *Science* 1997;276:575-9. DOI PubMed
32. Tamames-Tabar C, Cunha D, Imbuluzqueta E, et al. Cytotoxicity of nanoscaled metal-organic frameworks. *J Mater Chem B* 2014;2:262-71. DOI PubMed
33. Grall R, Hidalgo T, Delic J, Garcia-Marquez A, Chevillard S, Horcajada P. *In vitro* biocompatibility of mesoporous metal (III; Fe, Al, Cr) trimesate MOF nanocarriers. *J Mater Chem B* 2015;3:8279-92. DOI PubMed
34. Tang Z, Li X, Tong L, et al. A biocatalytic cascade in an ultrastable mesoporous hydrogen-bonded organic framework for point-of-care biosensing. *Angew Chem Int Ed Engl* 2021;60:23608-13. DOI PubMed
35. Bao Z, Xie D, Chang G, et al. Fine tuning and specific binding sites with a porous hydrogen-bonded metal-complex framework for gas selective separations. *J Am Chem Soc* 2018;140:4596-603. DOI PubMed
36. Tang J, Liu J, Zheng Q, et al. In-situ encapsulation of protein into nanoscale hydrogen-bonded organic frameworks for intracellular biocatalysis. *Angew Chem Int Ed Engl* 2021;60:22315-21. DOI PubMed
37. Liang W, Carraro F, Solomon MB, et al. Enzyme encapsulation in a porous hydrogen-bonded organic framework. *J Am Chem Soc* 2019;141:14298-305. DOI PubMed
38. Qin Z, Li H, Yang X, Chen L, Li Y, Shen K. Heterogenizing homogeneous cocatalysts by well-designed hollow MOF-based nanoreactors for efficient and size-selective CO_2 fixation. *Appl Catal B Environ* 2022;307:121163. DOI